A New Robust Control Scheme: Application for MPP Tracking of a PMSG-based Variable-speed wind turbine

Ali DALI[1], Samir ABDELMALEK[2*], Azzeddine BAKDI[3], Maamar BETTAYEB[4]

[1]Centre de Développement des Energies Renouvelables, CDER, BP 62 Route de l'Observatoire, Bouzaréah, Alger, 16340, Algérie;
Email: a.dali@cder.dz

[*2]Faculty of Technology, Department of Electrical Engineering, University of Medea, Algeria;
Email: samir_aut@yahoo.fr

[3]Department of Mathematics, University of Oslo, 0851 Oslo, Norway
Email: bkdaznsun@gmail.com

[4]Department of Electrical Engineering, University of Sharjah, United Arab Emirates, and Center of Excellence in Intelligent Engineering Systems (CEIES), King Abdulaziz University, Jeddah, KSA.
Email: maamar@sharjah.ac.ae

Abstract:

This paper proposes a novel Improved Maximum Power Point Tracking (IMPPT) algorithm to extract the maximum available power from a direct-drive Permanent-Magnet Synchronous Generator (PMSG) based standalone Small-scale Variable Speed Wind Turbine (VSWT). The proposed control scheme consists of an IMPPT algorithm to effectively improve the extracted power under various regimes of wind speed. The IMPPT constructs the reference value of the DC voltage for the DC bus. Moreover, a composite low-cost controller (LCC) is also proposed in order to improve the DC voltage tracking based on a new designed nonlinear state observer. The proposed nonlinear robust controller accounts for the overall system dynamics and nonlinear behavior. The objective is to improve the dynamic performance and ensure a good balance of energy conversion efficiency, robustness, cost efficiency, and a simple structure for practical implementation in wind energy conversion systems. Furthermore, the stability of the closed-loop system is analyzed and guaranteed through Lyapunov stability theory. Moreover, two scenarios are used for validation in Matlab/Simulink, including step change and stochastic profiles of wind speed. Simulation results verify the effectiveness and superiority of the IMPPT-LCC approach whereas comparisons with other techniques prove its superiority.

Keywords— Improved MPPT algorithm: Permanent-Magnet Synchronous Generator: Standalone Small-scale Wind Turbine: Robust sliding-mode controller: Nonlinear Observer: Low-cost controller.

Nomenclature

$\boldsymbol{A}$	The area covered by turbine blades (m^2)	$\boldsymbol{\Omega_t}$	The rotor speed (rad/s)
$\boldsymbol{\alpha}$	The switching control signal	$\boldsymbol{p}$	The number of pairs of poles
$\boldsymbol{C}$	The DC-DC converter capacitance (F)	$\boldsymbol{P_m}$	The aerodynamic power (W)
$\boldsymbol{C_p}$	The turbine-rotor-power coefficient	$\boldsymbol{P_{m_{opt}}}$	The optimal turbine power (W)
$\boldsymbol{C_{p_{opt}}}$	The optimal $\boldsymbol{C_p}$	$\boldsymbol{\psi_m}$	The PMSG the flux magnitude (Wb)
$\boldsymbol{e_1, e_2, e_3}$	The tracking errors	$\boldsymbol{\psi_s}$	The PMSG stator flux (Wb)
$\tilde{\boldsymbol{e}}_1, \tilde{\boldsymbol{e}}_2$	The observer tracking errors	$\boldsymbol{R}$	The wind turbine rotor radius (m)
$\boldsymbol{f_r}$	The viscous friction coefficient (N.m/s)	$\boldsymbol{\rho}$	The air density (kg/m^3)
$\boldsymbol{J}$	The turbine inertia ($kg.m^2$)	$\boldsymbol{R_s}$	The PMSG stator resistance (ohm)
$\boldsymbol{I_d}$	The input DC-DC converter current (A)	$\boldsymbol{r_L}$	The inductor resistance (ohm)
$\hat{\boldsymbol{I}}_{\boldsymbol{L}}$	The observer inductance (A)	$\boldsymbol{T_e}$	The electrical torque (N.m)
$\boldsymbol{I_{L_{ref}}}$	The inductor current reference (A)	$\boldsymbol{T_m}$	The wind turbine torque (N.m)
$\boldsymbol{i_s}$	The PMSG stator current (A)	$\boldsymbol{T_m^*}$	The wind turbine reference torque (N.m)
$\boldsymbol{k_1, k_2}$	Parameters of the proposed observer	$\hat{\boldsymbol{T}}_{\boldsymbol{m}}$	The estimated wind turbine torque (N.m)
$\boldsymbol{K_{opt}}$	The optimal power control gain	$\boldsymbol{u}$	the PWM duty cycle
$\boldsymbol{K_p, K_i}$	Parameters of the MPPT controller	$\boldsymbol{V_c}$	The input DC-DC converter voltage (V)
$\boldsymbol{L}$	The DC-DC converter inductance (H)	$\hat{\boldsymbol{V}}_{\boldsymbol{c}}$	The observer voltage (V)
$\boldsymbol{\lambda_1, \lambda_2, \lambda_3, \lambda_4}$	Parameters of the proposed controller	$\boldsymbol{V_{dc}}$	The DC link voltage (V)
$\boldsymbol{\lambda}$	The Tip Speed Ratio (TSR)	$\boldsymbol{V_{ref}}$	The reference voltage (V)
$\boldsymbol{\lambda_{opt}}$	The optimal TSR	$\boldsymbol{v_w}$	The wind speed (rad/s)
$\boldsymbol{L_s}$	The PMSG stator self-inductance (H)	$\boldsymbol{v_s}$	The PMSG stator voltage (V)
$\boldsymbol{\Omega_r}$	The electrical angular frequency (rad/s)		

Abbreviations

LCC	low-cost controller
MPPT	Maximum Power Point Tracking
IMPPT	Improved MPPT
MAE	Mean Absolute Error
PI	Proportional Integral
PMSG	Permanent-Magnet Synchronous Generator
PWM	Pulse Wave Modulation
P&O	Perturb and Observe algorithm
PSO	Particle Swarm Optimization
RESs	Renewable Energy Sources
SWT	Small-scale Wind Turbine
VSWT	Variable Speed Wind Turbine
TSR	Tip Speed Ratio
WECSs	Wind Energy Conversion Systems

1. Introduction

Nowadays, the population growth and the development of the economy imply a strong demand for energy where novel electrical power generation plants are required to meet the overall increasing energy needs. These developments fueled massive technological advances towards Renewable Energy Sources (RESs) which started to gain ground. The development of this type of energy makes a solution for reducing the dependency on fossil resources and, therefore, decreasing their negative impact on the environment. Wind energy is one of the most promising alternatives to ensure the goal of replacing fossil fuels, not only because its costs that continue to decline while the cost of fossil fuels continues to increase, but also to its unlimited resource advantage. Wind energy is a clean, non-polluting, reliable and widely available RES. The last decades exhibit massive increase in the installed wind capacity, wind turbine scale, and wind turbine market. In parallel, Small-scale Wind Turbines (SWTs) are becoming popular in standalone and grid-connected operations, especially in isolated locations. SWTs help their users to lower their electricity bills and avoid high costs due to over-extended power lines to remote locations and ensure an uninterruptible power source to avoid utility outages.

Over the last years, the most promising solution for variable-speed variable-pitch direct-drive Wind Energy Conversion Systems (WECSs) is based on the Permanent Magnet Synchronous Generator (PMSG) directly connected (no gearbox) to the turbine [1,2]. This solution is known for its advantages of high power density and efficiency with lower maintenance costs and increased reliability and grid support capability [3]. Recent research efforts focus on the development of converter prototypes, power and efficiency optimization, controller design, and grid-interface schemes to increase efficiency and reliability of WECSs. More importantly, since wind is a volatile unpredictable resource, it is of paramount importance that WECSs extract maximum possible power from the wind while it is available. Consequently, Maximum Power Point Tracking (MPPT) algorithms play a crucial role in WECSs and they are subject to continuous developments.

The overall WECSs are inherently complex processes involving interconnected aerodynamic, mechanical, and electrical parts [4], and integrating their unique characteristics which are difficult to model. PMSGs employed in WECSs involve different technologies from those in conventional synchronous generators [5]. Moreover, WECSs's PMSGs are fueled by wind, a volatile unpredictable resource. The wind speed model itself is complex and subject to many factors such as climate characteristics, geographic location, level above the ground, and surface topography [6]. Moreover, it is crucial to consider the entire operating range [7,8] for accurate WECS modelling and effective control design. To tackle the various MPPT and control problems over the whole wind speed range, the variable-speed variable-pitch wind turbine was modelled in [9] in the form of a linear parameter-varying system where a Gain-scheduled control strategy was exploited for effective pitch angle control in MPPT operations. The nonlinear model dynamics are also approximated by linearized models in [5,10] relating the active power output of WECS to the wind speed and network frequency deviations to reduce the system complexity through linear time-invariant models. Linear parameter-varying models are also adopted in [11] to approximate coupled nonlinear dynamics of the WECS. It was stated in [12] that the overall behavior of the WECS is nonlinear where improved linearized models are derived for better approximation using harmonic

linearization techniques. Linearised WECSs' models are advantageous in terms of their reduced complexity and offer deeper understanding of the system in the context of MPPT, however they remain local approximations of a very limited accuracy.

Due to the volatile and unpredictable wind speed, a great deal of research has been devoted in industry and academia to develop advanced MPPT search and control algorithms to reduce power losses in WECSs. The tradeoff between maximizing power output and minimizing mechanical damage was highlighted in[6] where semi-definite programming optimization technique was used for MPPT control using a linearized model of the WECS. A Perturb and Observe (P&O) algorithm was proposed in[13] for MPPT in WECSs where a sliding mode and Proportional Integral (PI) controllers are applied for PMSG and grid-side control. The downsides of P&O MPPT approaches are discussed in[14] where a self-adaptive P&O extension was proposed. However, it was reported in[15] that P&O-based MPPT algorithms exhibit a strong tradeoff between a slow convergence due to a small step size versus power oscillations for a large step size. Since the electrical components of the MPPT designs are subject to faults, [16] proposed a passive MPPT approach for standalone wind turbine generator systems.

WECSs's control has potential applications, and particularly in variable-speed wind turbines, to ensure the system stability, robustness, efficiency, and protection. [17] proposed an active power controller for variable-speed wind turbine for power oscillation damping during transient events using a derivative control that moves the operating point from MPPT to the virtual inertia control curves. [18] considered the problem of load control during extreme wind conditions. The problem of robust blade pitch control was addressed in[19] for periodic load disturbance rejection, whereas a feedforward fuzzy PID pitch controller was proposed in[20]. Adaptive fuzzy MPPT controller was also used in[21] for small-scale WECSs. A Grey-Wolf optimized PI fault-tolerant controller was proposed in[22] for low voltage ride through and MPPT in grid-connected MPSG driven by a variable speed wind turbine. [23] considered the problem of frequency control for the coordination of the PMSG in WECSs where a linear gain control was used. These linear controllers have basic structures and cannot satisfy multi-criteria that ensure efficiency and robustness together under MPPT. Different control strategies are compared in[24] for dynamic response of a floating wind turbine. Alternatively, nonlinear controllers are used instead of lienar controllers to address the nonlinearities of the system. [25] designed a neural networks identifier to approximate the mechanical torque in a wind turbine system from which a backstepping controller was developed. A sliding mode observer was used instead in[26] to estimate the aerodynamic torque which is used by a sliding mode controller to control the speed in a doubly-fed induction generator. In a closely related work, a discrete-time sliding mode controller was design in[27] as an observer to determine the reference value for the extractable power used by a sliding mode controller in a doubly-fed induction generator.

This paper presents the design of a new MPPT algorithm for a small-scale variable-speed wind turbine based standalone WECS based on a PMSG. The novel objective of the paper is to effectively improve the extracted power under various regimes of wind speed focusing simultaneously at multiple desired critea of dynamic tracking performance, robustness to uncertainties and disturbances, cost efficiency, and practical implementation. The exceptional novelties of the design are in the accurate fullest model of

the WECS and the consideration of stochastic wind speed, PMSG, and converter characteristics. More particularly, the proposed MPPT design constructs the reference value of the DC voltage for the DC, then a composite low-cost controller (LCC) is also proposed in order to improve the DC bus voltage tracking based on a new designed nonlinear state observer. The new composite design is advantageous for being robust and highly effective and it takes into account the nonlinearities of the system. The rest of this article is organized as follows: Section 2 gives a deeper understanding of the overall WECS and a complete model is derived for the nonlinear dynamics of its aerodynamic, mechanical, and electrical parts. Section 3 describes the main objectives of this work, the novel MPPT algorithm, the new nonlinear state observer, and the nonlinear controller. Validation scenarios are explained in Section 4 where the obtained results are compared and discussed. Finally, the major findings and potential applications of the proposed design are given in conclusions in Section 5.

2. System Modelling

This section gives a brief description of the overall wind energy conversion system. The structure of the PMSG-based SWT system, which mainly consists of three subsystems is presented in Fig. 1. It consists of an aerodynamic subsystem, a PMSG subsystem, and a DC-DC buck converter subsystem that relates to a stable DC link. The inverter is used in order to connect to AC loads.

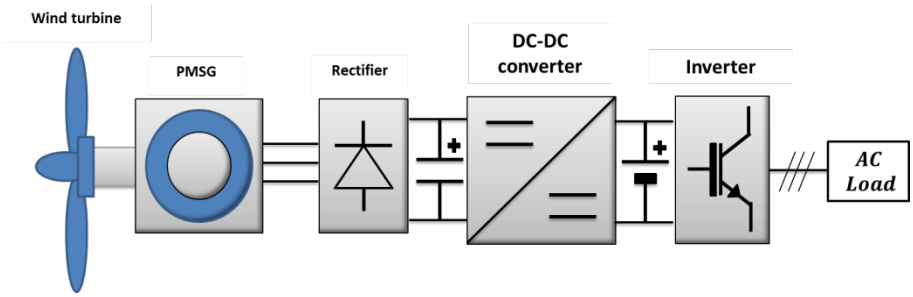

Fig. 1. Configuration of PMSG-based SWT system.

2.1. Aerodynamic modeling

The aerodynamic power P_m extracted from a wind turbine rotor can be expressed as a function of the rotor speed and wind speed [28,29]:

$$P_m = \frac{1}{2}\rho C_p(\lambda,\beta)A\, v_w^3, \tag{1}$$

where ρ is the air density, A is the area covered by turbine blades ($A = \pi R^2$), C_p is the turbine-rotor-power coefficient, β is the pitch angle and λ is the Tip Speed Ratio (TSR) defined as [31]:

$$\lambda = \frac{R\,\Omega_t}{v_w}, \tag{2}$$

where v_w is the wind speed, Ω_t denotes the rotor speed, and R represents the wind turbine rotor radius. Then, C_p can be described by the following equation [30,32]:

$$\begin{cases} C_p(\lambda) = 0.5\left(\frac{116}{\lambda_i} - 5\right)e^{-\frac{21}{\lambda_i}} + 0.01\lambda \\ \frac{1}{\lambda_i} = \left(\frac{1}{\lambda} - 0.03\right) \end{cases} . \quad . \tag{3}$$

The mechanical power curves generated by the turbine as a function of the rotor speed for different values of wind speed is depicted in Fig. 2.

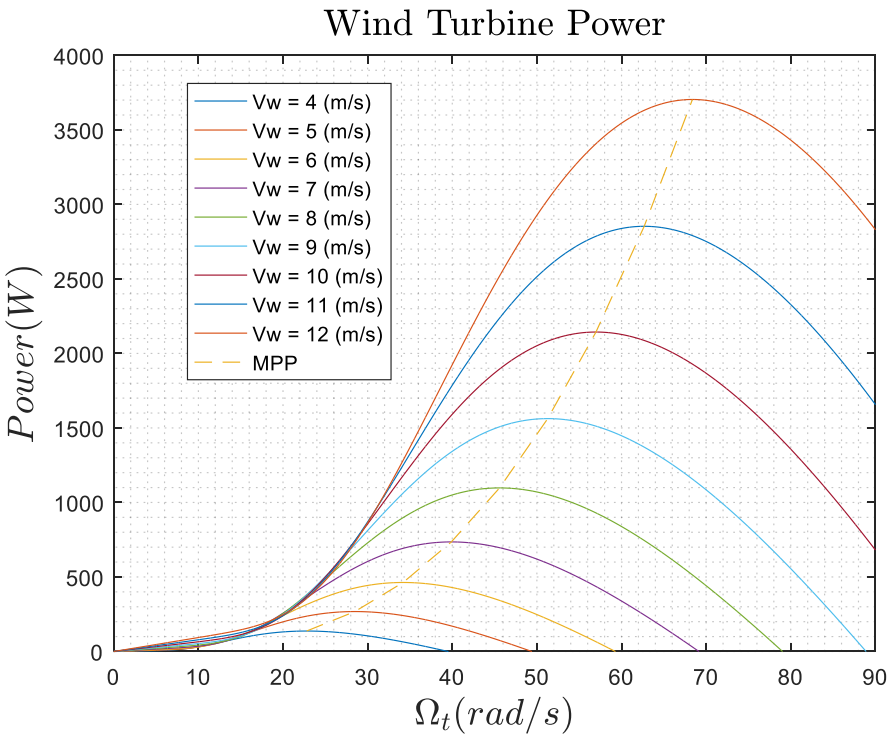

Fig. 2. Mechanical power generated by the turbine as a function of the rotor speed for different wind speeds.

The drive-train subsystem can be described as two lumped mass with torsion damping and stiffness system[8], which can be modeled as follows[33]:

$$T_m - T_e = J\frac{d\Omega_t}{dt} + f_r\,\Omega_t, \tag{4}$$

where f_r is the viscous friction coefficient, T_m denotes the wind turbine mechanical torque, T_e is the electrical torque, and J denotes the electrical machine and turbine inertia coefficient.
Rearranging Eq(4) yields to :

$$\frac{d\Omega_t}{dt} = \frac{T_m - f_r\Omega_t}{J} - \frac{T_e}{J}. \tag{5}$$

2.2. PMSG Dynamics

The stator dynamics of the PMSG can be described by the following dynamic equations [33]:

$$v_s = R_s i_s + \frac{d\psi_s}{dt}, \tag{6}$$

where v_s, i_s, ψ_s, R_s are, respectively, the stator voltage, stator current, stator flux, and the stator resistance. The stator flux linkage ψ_s is generated by the rotor magnets and the self-linked flux produced by the stator currents. This relation is described by[33]:

$$\psi_s = L_s i_s + \psi_m e^{j\theta} \tag{7}$$

through the stator self-inductance L_s, the flux magnitude ψ_m, and the rotor position θ.

$$v_s = R_s i_s + L_s \frac{di_s}{dt} + j\psi_m \Omega e^{j\theta}. \tag{8}$$

The stator equation of the PMSG can be rewritten in *d-q* coordinates as follows[33,34]:

$$\begin{cases} v_{sd} = R_s I_{sd} + L_s \dfrac{di_{sd}}{dt} - L_s \Omega_r i_{sq} \\ v_{sq} = R_s I_{sq} + L_s \dfrac{di_{sq}}{dt} + L_s \Omega_r i_{sd} + \psi_m \Omega_r \end{cases}, \tag{9}$$

where

$$\begin{cases} v_s = v_{sd} + j v_{sq} \\ i_s = i_{sd} + j i_{sq} \end{cases}, \tag{10}$$

where the electrical angular frequency (Ω_r) is given by [28]:

$$\Omega_r = p\, \Omega_t, \tag{11}$$

with the constant p refers to the number of pairs of poles.
The electric torque T_e depends on the flux magnitude and the quadrature component of the stator current vector [33]:

$$T_e = \frac{3}{2} p \psi_m i_{sq}. \tag{12}$$

2.3. DC-DC Buck Bonverter Dynamics Model

The topology shown in Fig. 3 is employed for controlling standalone wind turbines-based energy conversion systems [35], in which the input voltage or input current should track a desired reference in order to provide an optimal maximum power point tracking (MPPT) mode [36,37]. The switched model of the DC-DC buck converter is redefined through the average Pulse Wave Modulation (PWM) model [38,39]:

$$\begin{cases} C \dfrac{dV_c}{dt} = I_d - u I_L \\ L \dfrac{dI_L}{dt} = \alpha V_c - V_{dc} - r_L I_L \end{cases}, \tag{13}$$

where V_{dc} is the DC link voltage, I_d is the input current, and V_c is the input voltage which should be kept at a given constant value V_{ref}. L is the inductance, r_L is the inductor resistance, C is the capacitance and $\alpha \in \{0,1\}$ is the switching control signal that takes only binary values 0 (switch open) and 1 (switch closed).

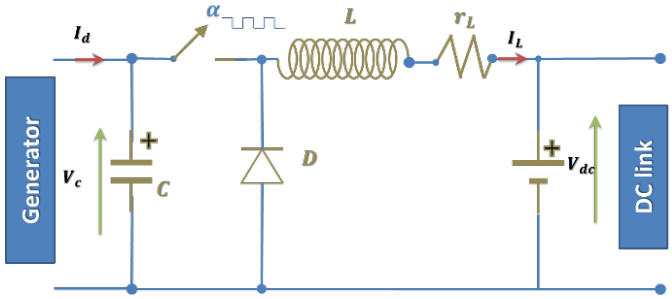

Fig. 3. Schematic diagram of the DC-DC buck converter**.**

In order to achieve a zero steady-state error in the output voltage, the integral term of the output voltage is added as a new state variable x_1 to Eq(13), which increases the order of Model Eq(13). Then, the resulting augmented model is given as:

$$\begin{cases} \dfrac{dx_1}{dt} = V_c \\ C\dfrac{dV_c}{dt} = I_d - uI_L \\ L\dfrac{dI_L}{dt} = uV_c - V_{dc} - r_L I_L \end{cases}, \tag{14}$$

where u represents the PWM duty cycle, and the state vector x is given as:

$$x = \left[\int V_c \quad V_c \quad I_L\right]^T. \tag{15}$$

3. Problem Formulation and Novel Designs

The principal objective of the control is to maximize the extracted power from wind and keeping the PMSG-based turbine at its optimal speed. These objectives are guaranteed by the control of the DC-DC converter. In this regard, a novel improved MPPT algorithm and a composite low-cost nonlinear control strategy are proposed in this section. The overall strategy consists of:

1. An Improved MPPT (IMPPT) algorithm design which permits to improve the maximum power point tracking from the SWT. This algorithm constructs the optimal DC voltage (V_{ref}) value that should be tracked.
2. A new nonlinear controller design which provide an effective and smooth tracking of the desired voltage (V_{ref}) in order to ensure the maximum power extraction.
3. A novel nonlinear state-observer is designed to estimates the inductor current (I_L) of the DC-DC converter. This estimation of I_L will be used in the controller design.

Therefore, this section is divided into three subsections. The first subsection briefly presents the proposed MPPT algorithm. Then, the second subsection describes the whole design procedure for the proposed nonlinear controller. The last subsection presents the proposed nonlinear state-observer design. The schematic diagram of the proposed control strategy is shown in Fig. 4.

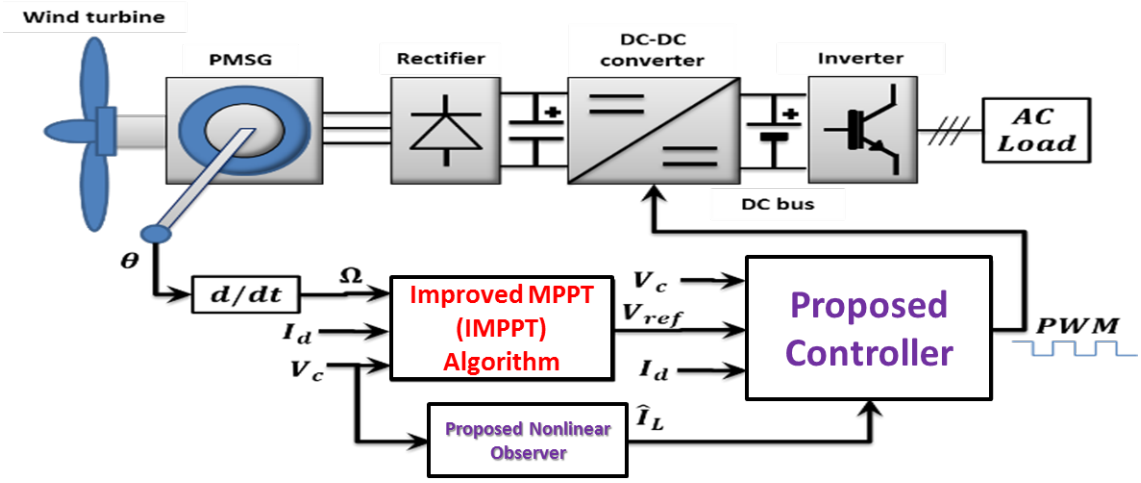

Fig. 4. Block diagram of the proposed control strategy.

3.1. A New Improved MPPT (IMPPT) Algorithm

MPPT algorithms are used to search for the optimal operating point in wind energy conversion systems. The main aim of these algorithms is to extract the maximum electrical power generated from the small-scale wind turbines (SWT) by tracking the optimal wind turbine speed which allows an optimal TSR (λ_{opt}) [40]. From this purpose, a great deal of research effort is devoted to develop new MPPT search algorithms in order to improve the convergence speed to the optimum, to avoid local minima, and minimize power oscillations of the existing MPPT algorithms. An improved MPPT algorithm is proposed herein to effectively extract maximum power from the PMSG-SWT and improve convergence speed and accuracy compared to conventional MPPT algorithms.

When the turbine-rotor-power coefficient C_p is at its optimum value $C_{p_{opt}}$, the SWT produces the maximum power. Therefore, it is important to keep the rotor speed at an optimum value of the tip-speed ratio λ_{opt}. While the wind speed varies, the rotor speed should be adjusted in order to follow this change [33]. Then, the optimum power ($P_{m_{opt}}$) that can be extracted from a SWG and the optimal TSR can be defined, respectively, as follows [39] :

$$\begin{cases} P_{m_{opt}} = \dfrac{1}{2}\,\rho\, C_{p_{opt}} A\, v_w^3 \\ \lambda_{opt} = \dfrac{R\Omega_{opt}}{v_w} \end{cases}, \tag{16}$$

where Ω_{opt} represents the optimum SWT rotation speed.

The optimum generator power $P_{m_{opt}}$ and the target optimum torque $T_{m_{opt}}$ can be calculated respectively, as [40]:

$$\begin{cases} P_{m_{opt}} = K_{opt}\Omega_{opt}^3 \\ T_{m_{opt}} = K_{opt}\Omega_{opt}^2 \end{cases}, \tag{17}$$

where the optimal power control gain K_{opt} can be described as:

$$K_{opt} = \frac{1}{2}\,\rho\, C_{p_{opt}} A \left(\frac{R}{\lambda_{opt}}\right)^3. \tag{18}$$

The wind speed measurement is not required and the optimum power is simply reached by maintaining the wind turbine torque at its optimum value:

$$T_m^* = K_{opt}\Omega_t^2, \tag{19}$$

where T_m^* represents the WT reference torque value.

The estimated WT torque ($\hat{T}_m$) can be calculated as:

$$\hat{T}_m = \frac{V_c I_d}{\Omega_t}, \tag{20}$$

where I_d and V_c are, respectively, the current and the voltage at the output of the rectifier.

A block diagram summarizing the proposed MPPT algorithm is depicted in Fig. 5.

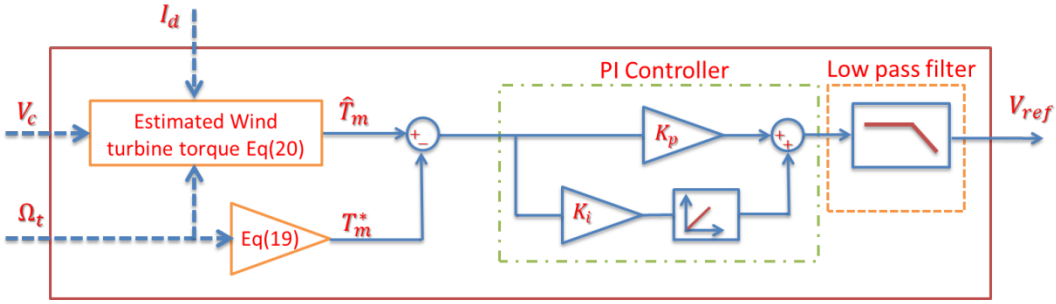

Fig. 5. Block diagram of the proposed MPPT algorithm.

The overall design procedure of the proposed IMPPT control algorithm can be summarized in the following steps:

Proposed IMPPT Algorithm	
Step 1:	Measure the generator speed (Ω_t)
Step 2:	Determine the reference torque T_m^* of the WT according to Eq(19)
Step 3:	Calculate the estimated WT torque $\hat{T}_m$ via the measured values of the current and the voltage at the output of the rectifier (I_d and V_c) using Eq(20)
Step 4:	The PI controller is used to enhance and improve the tracking speed performance
Step 5:	The low pass filter is used to ensure a smooth reference output voltage V_{ref}

3.2. Composite Nonlinear Controller Design

The main objective here is to design a control law to force the measured output voltage V_c for the DC-DC buck converter to track efficiently, and in a finite time, the desired output voltage trajectory (V_{ref}) generated by the IMPPT algorithm presented previously. We proceed with the control design:

1. Define the tracking errors;
2. Select the sliding surfaces;
3. Determine a control Law which forces the trajectory of the system state to the predefined sliding surfaces defined in previous step;

3.2.1. Tracking Errors Definition

In the first time, let us define the integral output voltage tracking error (e_1):

$$e_1 = -\int \left(V_c - V_{ref}\right)\, dt. \tag{21}$$

Then, the output voltage tracking error (e_2) is:

$$e_2 = V_{ref} - V_c, \tag{22}$$

and the current tracking error (e_3):

$$e_3 = I_{L_{ref}} - I_L, \tag{23}$$

where $I_{L_{ref}}$ denotes the reference current generated by the voltage loop controller and V_{ref} denotes the desired output voltage of the DC-DC buck converter.

According to Eq(14), Eq (21), Eq (22), and Eq (23),

the time derivative of the integral output voltage tracking error (e_1) can be derived as

$$\dot{e}_1 = V_c - V_{ref} \tag{24}$$

The error dynamics of e_2 are given by

$$\dot{e}_2 = -\dot{V}_c. \tag{25}$$

The time derivative of the current tracking error (e_3) yields

$$\dot{e}_3 = \dot{I}_{L_{ref}} - \dot{I}_L, \tag{26}$$

with the reference current $I_{L_{ref}}$ given by

$$I_{L_{ref}} = \xi e_1 + \eta\, e_2 + \gamma, \tag{27}$$

with,

$$\begin{cases} \xi = -\dfrac{C}{u}(1+\lambda_1\lambda_2) \\ \eta = -\dfrac{C}{u}(\lambda_1+\lambda_2)\ , \\ \gamma = \dfrac{I_d}{u} \end{cases} \tag{28}$$

where λ_1 and λ_2 are real positive numbers.

Three sliding surfaces are designed according to the number of state variables as in Eq(14).

3.2.2. Sliding Surfaces Selection

In this study, the proposed sliding surfaces $S(e_1, e_2, e_3)$ are selected as [45]:

$$S(e_1, e_2, e_3) = \begin{bmatrix} e_1 \\ \lambda_1 e_1 + e_2 \\ \Upsilon e_3 \end{bmatrix}. \tag{28}$$

with $\Upsilon = \sqrt{\frac{L}{C}}$.
Then, the control law (u) of Eq(33) ensures the stability of the system of Eq(14).

Proof. In order to demonstrate the theoretical convergence of the proposed control strategy, let's define the following Lyapunov candidate function

$$V(\,e_1, e_2, e_3) = \tfrac{1}{2} S^2(\,e_1, e_2, e_3). \tag{29}$$

In order to satisfy the reaching conditions of sliding mode, the control input must therefore ensure the following condition [41]:

$$\dot{V}(\,e_1, e_2, e_3) < 0 \ \Rightarrow\ S(\,e_1, e_2, e_3)\,\dot{S^T}(\,e_1, e_2, e_3) < 0. \tag{29}$$

According to Eqs(24)-(28) and Eq(29), the time derivative of V, along the trajectories of Eq(14), gives

$$\begin{aligned} S\dot{S}^T = e_1 e_2 + (e_2 + \lambda_1 e_1)\left(-\frac{1}{C}(I_d - uI_L) + \lambda_1 e_2\right) \\ + e_3\left(\dot{I}_{L_{ref}} - \frac{1}{L}(uV_c - V_{dc} - r_L I_L)\right). \end{aligned} \tag{30}$$

Adding and subtracting the term $(\lambda_1 e_1)$ to the previous equation $(e_1 e_2)$, with some mathematical developments, yields to:

$$S\dot{S}^T = -\lambda_1 e_1^2 + (e_2 + \lambda_1 e_1)\left(e_1 + \frac{u}{C} I_{L_{ref}} - \frac{1}{C}(I_d + u e_3) + \lambda_1 e_2\right) + \frac{L}{C} e_3 \left(\dot{I}_{L_{ref}} - \frac{1}{L}(u V_c - V_{dc} - r_L I_L)\right). \quad (31)$$

Replacing Eq(27) into Eq(31), gives

$$S\dot{S}^T = -\lambda_1 e_1^2 - \lambda_2 (e_2 + \lambda_1 e_1)^2 + e_3 \left(\frac{L}{C}\dot{I}_{L_{ref}} - \frac{1}{C}(u V_c - V_{dc} - r_L I_L) - \frac{u}{C}(e_2 + \lambda_1 e_1)\right). \quad (32)$$

3.2.3. Control Law Determination

From the previous mathematical manipulation, the resulting control law (u) can be derived as:

$$u = \frac{\tau(V_{dc} + r_L I_L)}{C} + \frac{L\tau}{C}\dot{I}_{L_{ref}} + \lambda_3 \tau\, e_3 + \lambda_4 \tau\, sign(e_3), \quad (33)$$

with $\tau = \frac{C}{(V_{ref} + \lambda_1 e_1)}$.

According to Eq(32) and Eq(33), thus

$$\dot{V} = -\lambda_1 e_1^2 - \lambda_2 (e_2 + \lambda_1 e_1)^2 - \lambda_3 e_3^2 - \lambda_4 |e_3| < 0. \quad (34)$$

Based on Eq(32), it can be concluded that the proposed nonlinear controller can converge within a finite time according to the Lyapunov stability theory.

3.3. Proposed Nonlinear Observer Design

This subsection proposes a nonlinear state observer as a tool to manage the cost for the PMSG-based SWT. This observer estimates the inductor current (I_L), then, the resulting estimation will be investigated for the design of the low-cost nonlinear controller presented in the previous subsection.
First, the following state estimation errors are defined as

$$\begin{cases} \tilde{e}_1 = \hat{V}_c - V_c \\ \tilde{e}_2 = \hat{I}_L - I_L \end{cases}. \quad (35)$$

Then, the dynamical equations of the proposed observer are

$$\begin{cases} \frac{d\hat{V}_c}{dt} = \frac{1}{C}\left(I_d - u\hat{I}_L + k_1 \tilde{e}_1\right) \\ \frac{d\hat{I}_L}{dt} = \frac{1}{L}\left(-V_{dc} - r_L \hat{I}_L + u\hat{V}_c + k_2 u\, \tilde{e}_2\right) \end{cases}. \quad (36)$$

According to Eq(20), Eq(35) and Eq(36), the error dynamics of Eq(35) can be obtained as

$$\begin{cases} \dot{\tilde{e}}_1 = \frac{1}{C}(k_1\tilde{e}_1 - u\tilde{e}_2) \\ \dot{\tilde{e}}_2 = \dfrac{1}{L}(-r_L\tilde{e}_2 + u(\tilde{e}_1 + k_2\tilde{e}_1)) \end{cases}. \tag{37}$$

From Eq(37) with selecting $k_2 = -1$, Eq(36) becomes

$$\begin{cases} \dot{\tilde{e}}_1 = \frac{1}{C}(k_1\tilde{e}_1 - u\tilde{e}_2) \\ \dot{\tilde{e}}_2 = -\dfrac{r_L}{L}\ \tilde{e}_2 \end{cases} \tag{38}$$

Proof. The convergence proof of the proposed observer is made with the Lyapunov theory, the following Lyapunov candidate function is considered:

$$P = P_1 + P_2, \tag{39}$$

with

$$\begin{cases} P_1 = \dfrac{L}{2}\hat{z}_2^2 \\ P_2 = \dfrac{C}{2}(\hat{z}_1 - \psi\ \hat{z}_2)^2 \end{cases}, \tag{40}$$

where $\psi = \frac{u}{r_L C/L + k_1}$.

The derivative of the Lyapunov candidate function is

$$\dot{P} = -r_L\hat{z}_2^2 + k_1(\hat{z}_1 + \psi\ \hat{z}_2)(\hat{z}_1 - \psi\hat{z}_2). \tag{41}$$

Then, the derivative of Lyapunov function P as in Eq(41) is negative definite by choosing the value of k_1 sufficiently small, it is therefore possible to get a convergence in a finite time.

4. Simulation and Discussion of Results

In order to demonstrate the effectiveness and the performance of the improved MPPT algorithm (IMPPT) with the new composite low-cost robust controller (LCC). The proposed design (IMPPT-LCC) is compared throughout this study with some other techniques such as a the improved IMPPT based PI controller tuned with PSO algorithm (IMPPT-PI-PSO), the MPPT algorithm proposed in [33] referred to as (MPPT) with a new LCC (MPPT-LCC) and with a PI-PSO (MPPT-PI-PSO). This makes four MPPT-controller design candidates into the comparison: IMPPT-LCC, IMPPT-PI-PSO, MPPT-PI-PSO and MPPT-LCC. Moreover, two different validation scenarios are conducted in a simulation study with Matlab/Simulink, including consecutive step changes and stochastic wind speed profiles.

Table 1. Main parameters of the DC-DC buck converter.

Parameters	Value
R_L	0.2Ω
V_{dc}	$400V \mp 10V$
C	$500\mu F$
L	$200\mu H$
I_d	$10\ A$
V_{dc}	$96\ V$

Table 2. Parameters of the PMSG-based SWT with 3.5-kW.

Wind Turbine	
Air density	1.225 Kg/m^3
Area covered by turbine	7.06 m
Optimum Coefficient K_{opt}	11.6 10^{-3} Nm/(rad/s)
Maximum power Coefficient $C_{\max}$	0.4951
Base wind speed	12 m/s
PMSG	
Stator resistance	0.6 Ω
Stator self-inductance	2.5 mH
Flux magnitude	0.34 Wb
Number of pole pairs	8

The parameters used for the simulation study are listed in the Table 1 and Table 2. The tuned parameters of the proposed low-cost controller are all listed in Table 3; whereas the parameters of the proposed IMPPT and the conventional MPPT algorithms are tuned by PSO algorithm (for more deatails see[46]) and are also given in Table 4.

Table 3. Controller gains.

Controller	**Notations**	**Gains**
Tuned-PI controller (PI-PSO)	k_P	0.5
(**for comparasion**)	k_i	0.02
	k_1	200
Proposed nonlinear controller	k_2	10
(**Subsection 2.2**)	k_3	1000
	k_4	80
Proposed nonlinear observer	λ_1	-0.5
(**Subsection 2.3**)	λ_2	1

Table 4. Parameters of the proposed IMPPT algorithm.

MPPT algorithms	Notations	Gains
Proposed IMPPT	k_P	13.2
(**Section 2.1**)	k_i	40

The Matlab/Simulink model developed to simulate the proposed control strategies is shown in Fig. 6 which gives an implementation overview on the proposed approach.

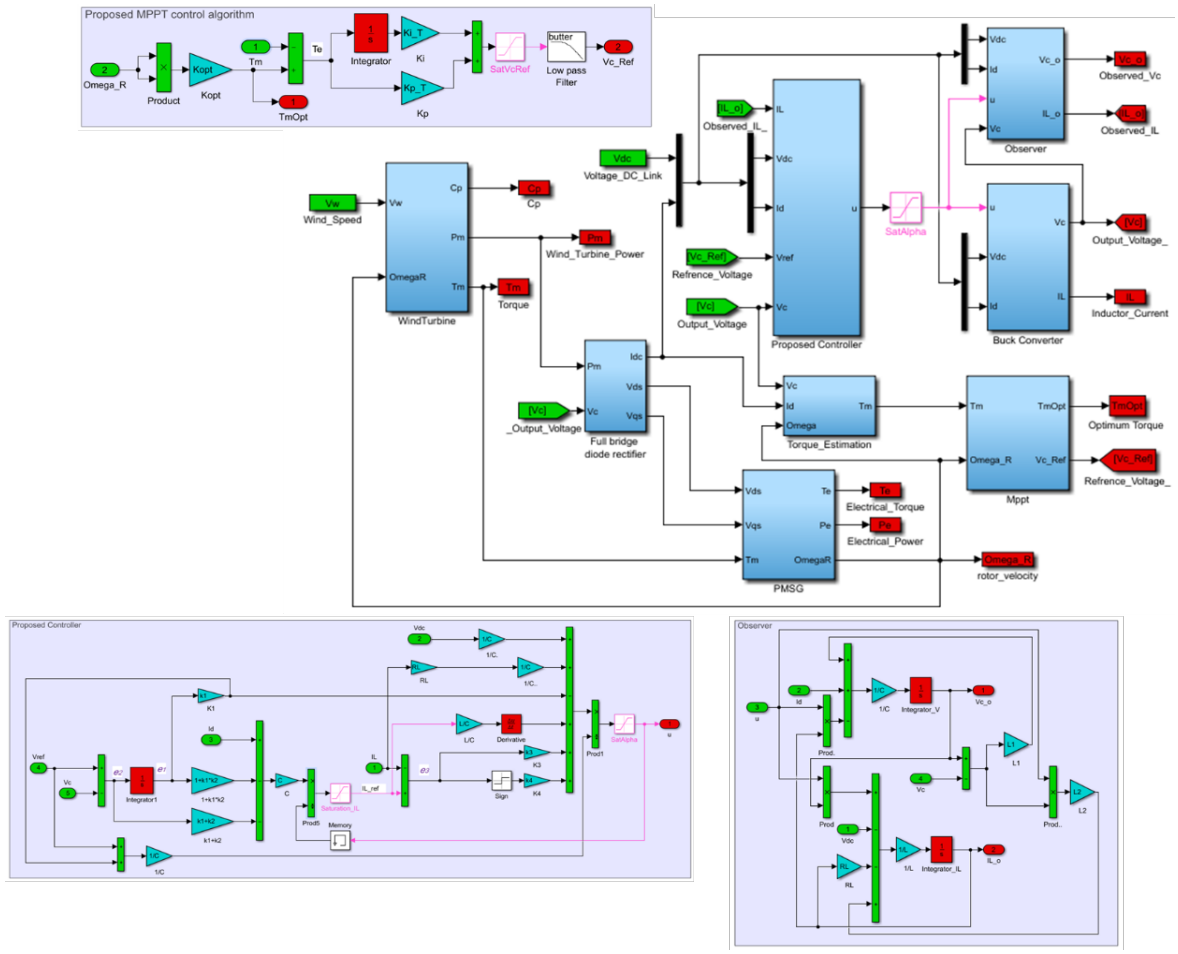

Fig. 6. Simulation model of the controlled system with the proposed controllers in Matlab/Simulink.

4.1. Step Wind-Speed Change

In this scenario, the applied wind speed includes five consecutive abrupt step-changes; the wind speed varies between 9 m/s to 12 m/s, as shown in Fig. 7.

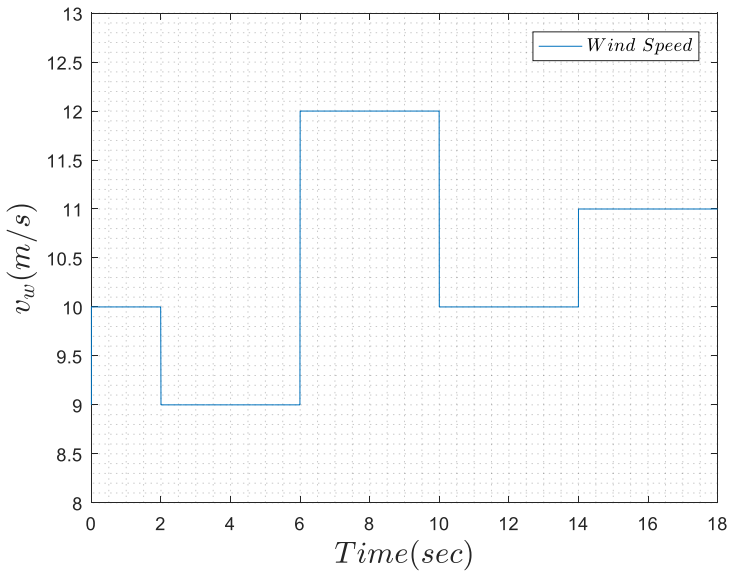

Fig. 7. Wind speed profile for five consecutive step-changes profile.

The responses comparisons obtained by the PMSG-SWT with the proposed and other MPPT control strategies are shown in Figs. 8 and 9, respectively.

- It can be seen from Fig.8(a) that the proposed IMPPT-LCC outperforms the other techniques, the correspoding energy produced is 42.6 kJ. Compared to that, energy losses are 3.5J for the IMPPT-PI-PSO, 92.1 J for the MPPT-LCC, and 93.3 J for the MPPT-PI-PSO as listed in Table 5. Furthermore, for statistic comparison, a mean absolute error (MAE) criterion is used for comparisons of the presented methods and the corresponding results are summarized in Table 5.
- Fig.8(b) depicts the power point coefficient of the SWT with different MPPT strategies. It can be observed that the proposed IMPPT-LCC strategy achieves a maximum power point coefficient of 0.49 besides the minimum oscillation losses as compared to the other three strategies.
- Fig.8(c) demonstrates that the wind turbine rotation speed follows the optimum established speed more effectively and rapidly through the IMPPT-LCC compared to the other control strategies. The corresponding time performances of all the methods are summarized in Table. 5. Also, Figs. 8(d) depicts the mechanical torque which tracks the optimum theoretical torque with the proposed IMPPT-LCC at a higher accuracy compared to the other control strategies.
- Therefore, this analysis demonstrates that the proposed IMPPT-LCC ensures a higher efficiency and improved reliability in the tracking maximum available power from the PMSG-SWT.

Table 5. Performance comparison under five consecutive step-change profiles.

MPPT Technique	**Response time (sec)**				**Control Technique**	**MAE** = $\frac{1}{n}\sum_1^n\lvert V_{ref} - V_c\rvert$	**Energy lost (joules)**
	[t=2]	**[t=6]**	**[t=10]**	**[t=14]**			
IMPPT	**0.095**	**0.169**	**0.168**	**0.103**	LCC	**0.15**	-
							3.5
MPPT	0.401	0.790	0.410	0.406	PI-PSO	0.34	92.1
							93.3

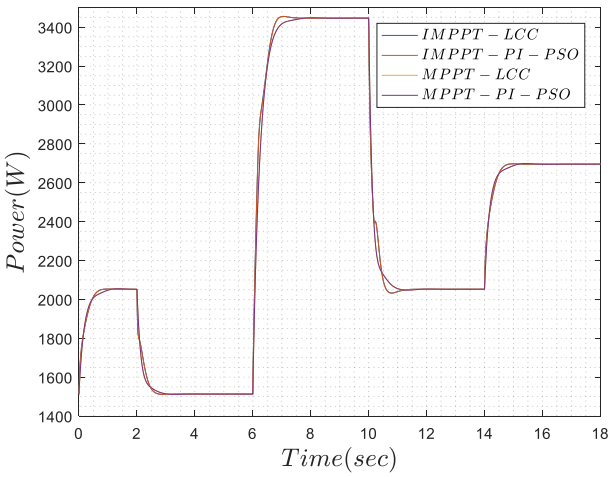

(a) Responses of SWT power

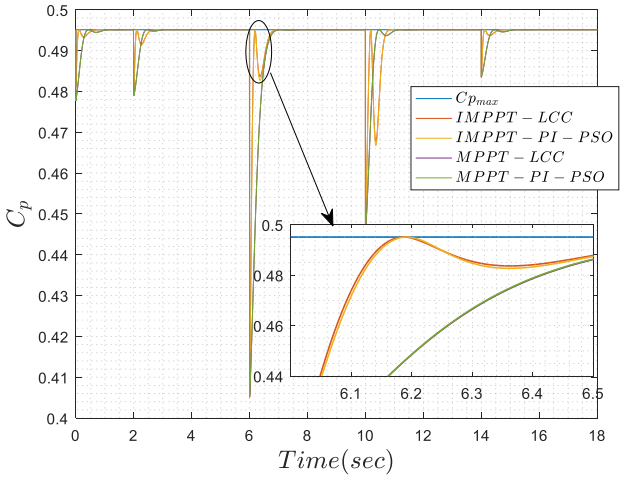

(b) Responses of SWT power coefficient

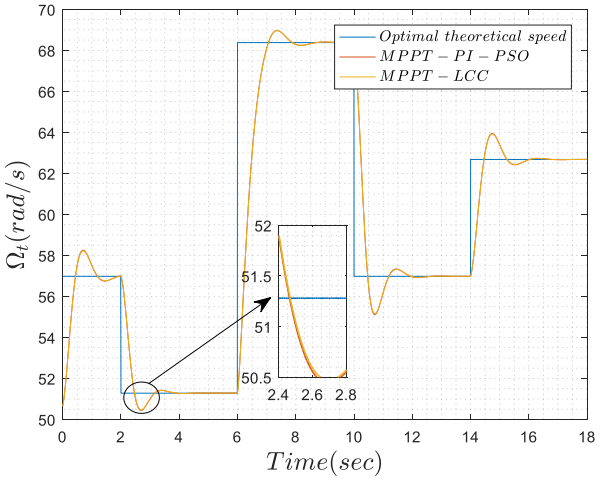

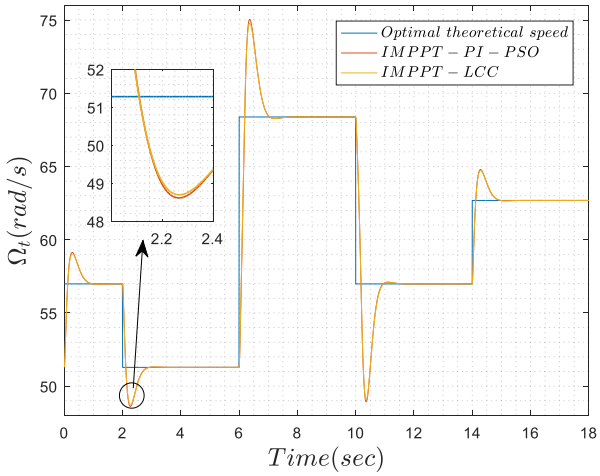

(c) Responses of SWT rotor speed

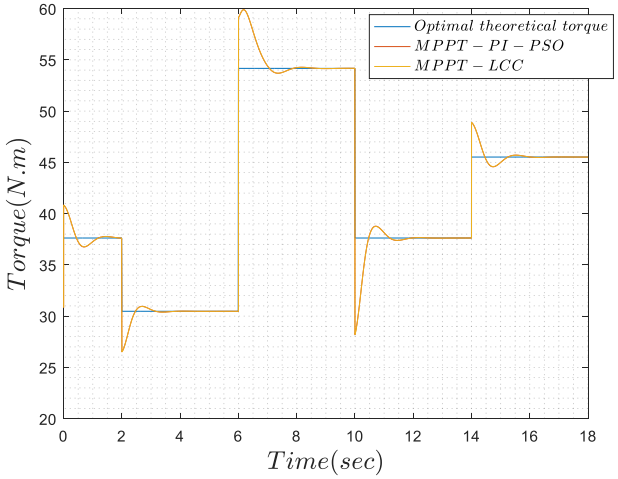

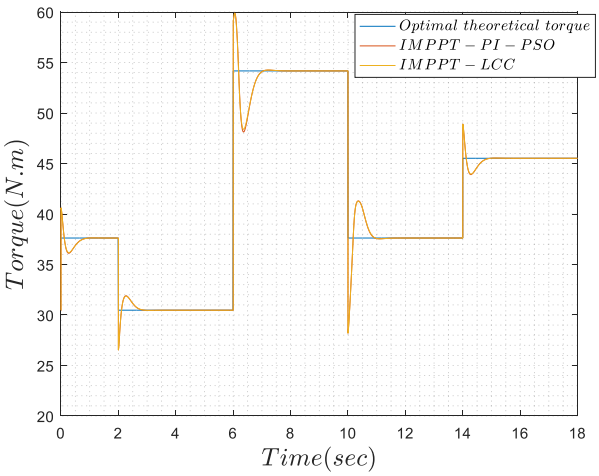

(d) Responses of SWT torque

Fig. 8. Performance comparison across the improved MPPT based on the proposed controller, the MPPT based on PI-PSO controller, the conventional MPPT based on the proposed controller, and the conventional MPPT based on PI-PSO controller.

- It can be seen from Fig. 9 that the proposed IMPPT-LCC approach permits to track smoothly the desired output voltage of the DC-DC buck converter compared to the PI-PSO controller.

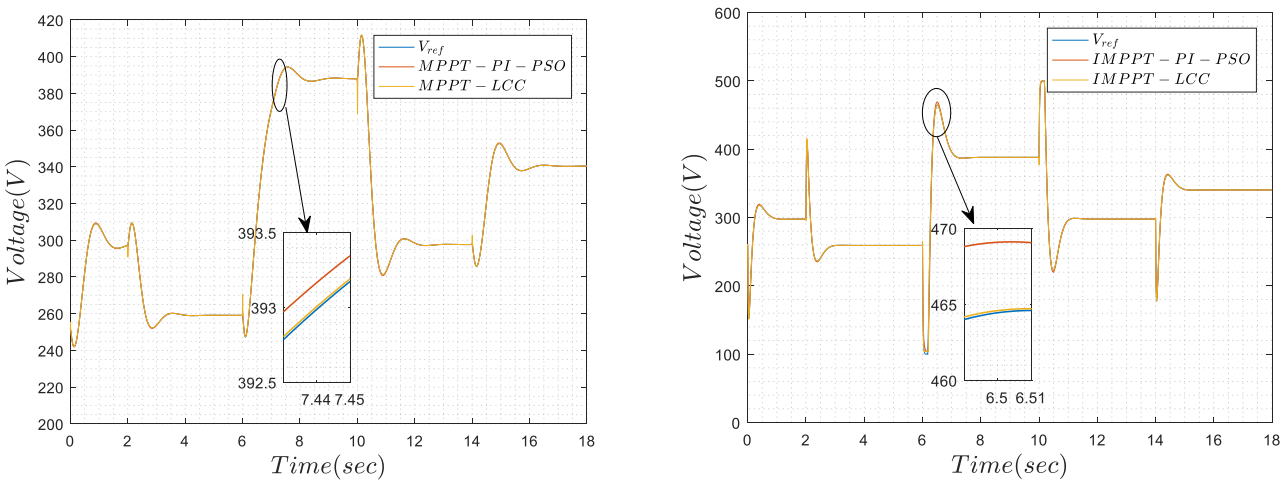

(a) **(b)**

Fig. 9. Performance comparison of the output voltage tracking using the improved MPPT based on the proposed controller, the improved MPPT based on PI-PSO controller, the conventional MPPT based on the proposed controller, and the conventional MPPT based on PI-PSO controller.

4.2. Stochastic Wind Speed Variation

Under the imposed wind speed profile shown in Fig. 10, the dynamic responses of the PMSG-SWT with different control strategies are shown in Figs. 11 and 12. These results are also listed in Table 6.

We can observe that the proposed IMPPT-LCC has also better efficiency, the proposed strategy is superior in terms of energy production with 43.1 kJ which proves it superiority in tracking and extracting the maximum available power from the PMSG-SWT in cases of stochastic wind speed profiles. These results demonstrate the superiority of the proposed IMPPT-LCC compared to the other presented MPPT and control techniques.

- In terme of energy lost : the energy produced using IMPPT-LCC technique reached 43.1 kJ. Compared to that, energy losses are 1.0 J for the IMPPT-PI-PSO, 194.5 J for the MPPT-LCC and 93.3 J MPPT-PI-PSO.
- In terms of energy lost: the energy produced using IMPPT-LCC technique reached 43.1 kJ. Compared to that, energy losses are 1.0 J for the IMPPT-PI-PSO, 194.5 J for the MPPT-LCC and 93.3 J MPPT-PI-PSO.
- In terms of optimal tracking of the desired reference, the mean absolute error (MAE) criterion indicates also that the LCC technique allow better tracking compared with the PSO -PI technique.
- In terms of maximum power tracking, the proposed IMPPT-LCC strategy achieves a maximum power point coefficient of 0.49 faster and with minimum oscillation compared to the other three strategies.

The ability of the proposed technique is specially obtained by considering the nonlinear nature of the DC-DC converter while designing the voltage controller which allowed a better reference tracking. On the other hand, the proposed IMPPT allows to get the optimum power by improving the convergence time.

In addition, the designed observer allows us to avoid additional cost of the current but also, it is can be further investigated for sensor and actuator faults control [28,42-44] and fault detection and isolation.

Table 6. Performance comparison under a stochastic wind speed profile.

MPPT Technique	**Control Technique**	**MAE** = $\frac{1}{n}\sum_{1}^{n}\left\|V_{ref}-V_c\right\|$	**Energy lost (joules)**
IMPPT	LCC	**0.1581**	**-**
			1.0
MPPT	PI-PSO	0.3983	194.5
			194.5

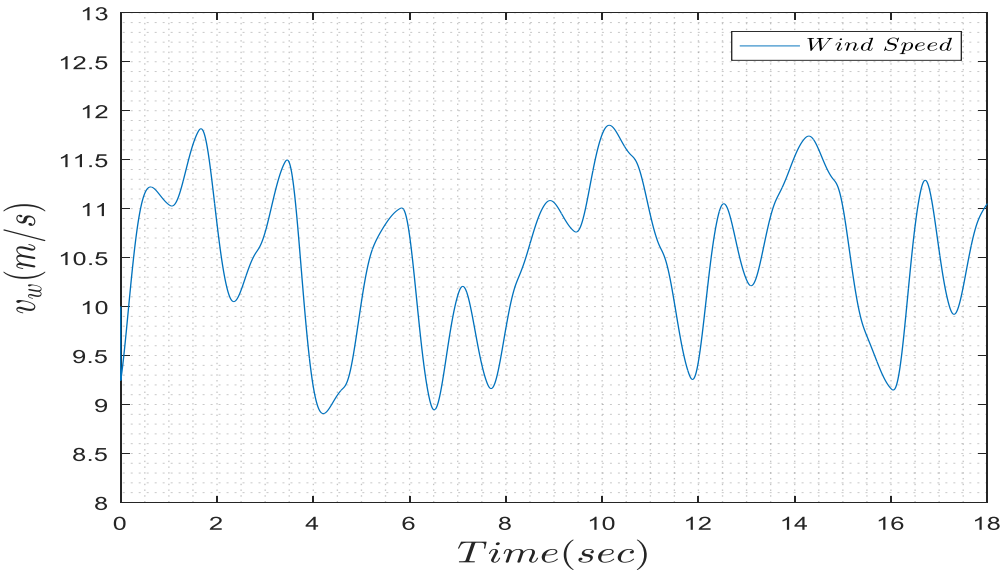

Fig. 10. Stochastic wind speed profile.

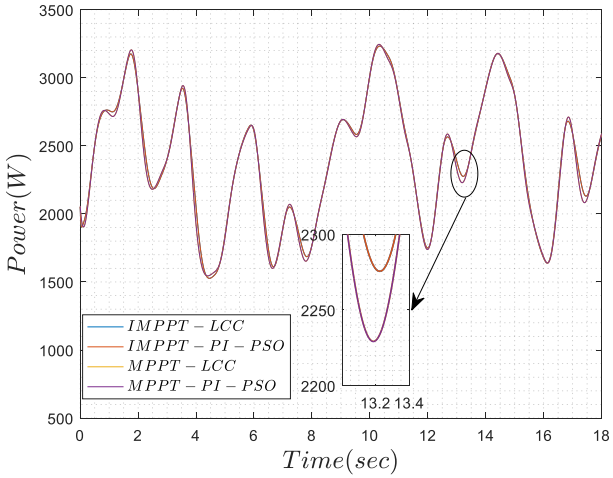

(a) Responses of SWT power

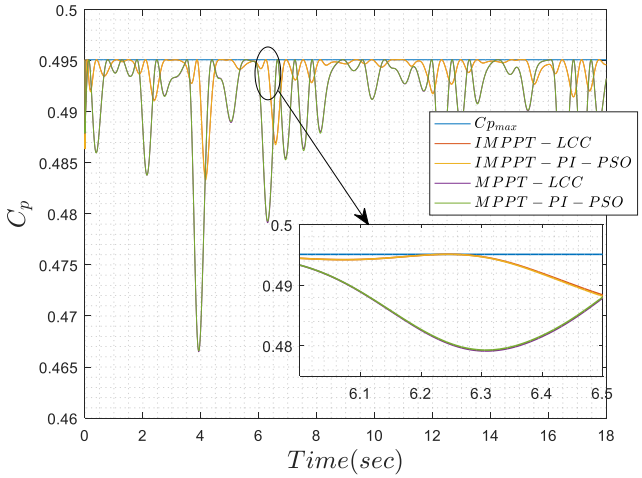

(b) Responses of SWT power coefficient

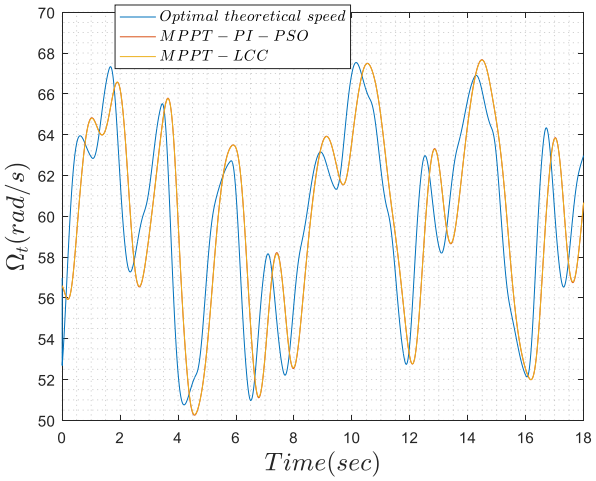

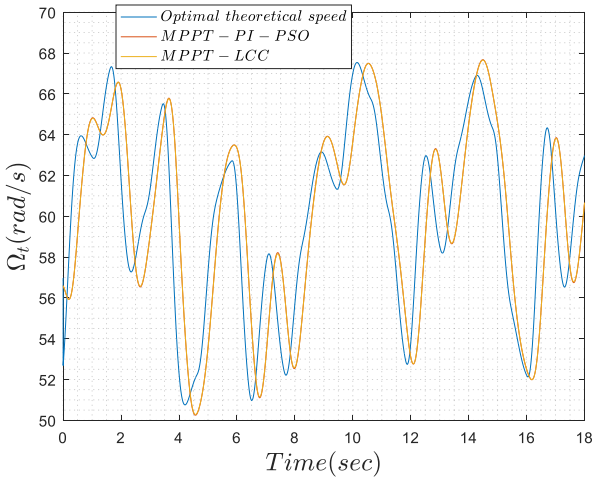

(c) Responses of SWT rotor speed

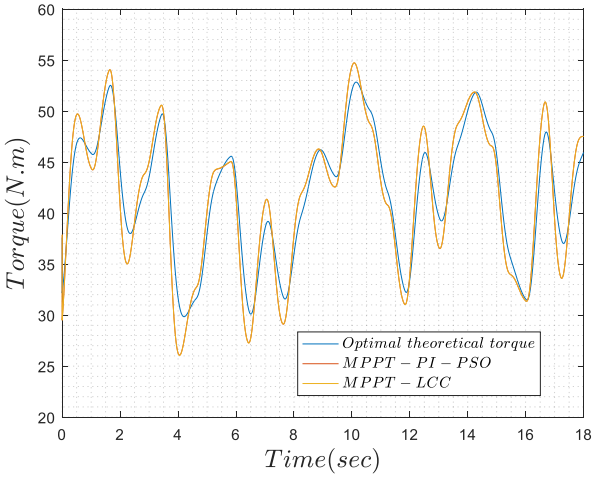

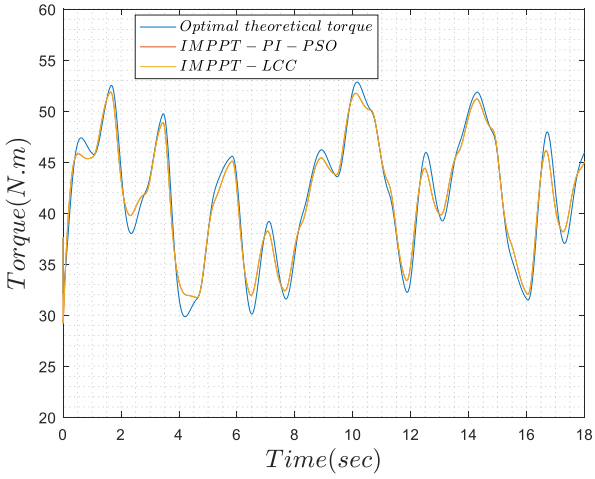

(d) Responses of SWT torque

Fig. 11. Performance comparison using the improved MPPT based on the proposed controller, the improved MPPT based on PI-PSO controller, the conventional MPPT based on the proposed controller, and the conventional MPPT based on PI-PSO controller.

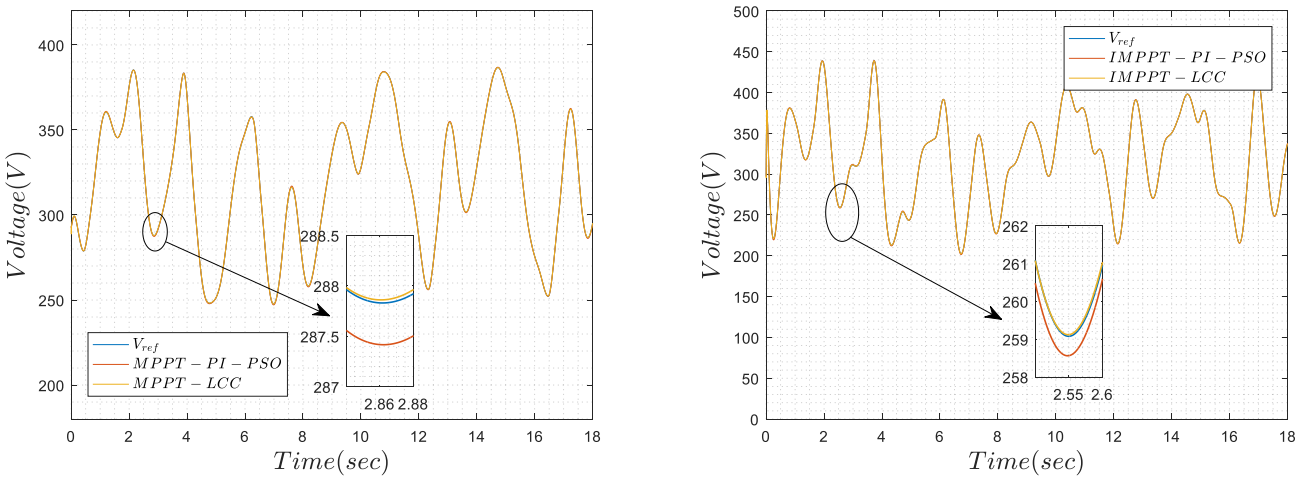

Fig. 12. Performance comparison of the output voltage tracking using the improved MPPT based on the proposed controller, the improved MPPT based on PI-PSO controller, the conventional MPPT based on the proposed controller, and the conventional MPPT based on PI-PSO controller.

5. Conclusion

A novel improved MPPT algorithm was presented in this work for extracting the maximum available power in wind energy conversion systems. A composite low-cost control strategy for PMSG-small-scale standalone wind turbine was also proposed in this study. Our new strategy accounted for the overall system dynamics and nonlinear behaviour. Stability and tracking analyses of the whole closed-loop system are demonstrated based on Lyapunov theory. Furthermore, the performance of the proposed IMPPT-based LCC are evaluated and compared with contemporary MPPT control techniques in Matlab/Simulink under different test scenarios. The obtained results proved that the proposed IMPPT-LCC has effectively increased both reliability and efficiency in tracking the maximum available power from the PMSG-SWT and it improved the output voltage tracking in the DC bus of the power source. The proposed strategy showed the capability to maximize the produced energy from SWTs through the low-cost simple controller which has a remarkable advantage in practical implementations. Future work will consider investigating the proposed control scheme to intelligent fault detection and fault tolerant control applications.

References

[1]. N. A. Orlando, M. Liserre, R. A. Mastromauro, Dell'Aquila, A survey of control issues in PMSG-based small wind-turbine systems, IEEE transactions on Industrial Informatics, 9(3) (2013) 1211-1221. DOI: 10.1109/TII.2013.2272888.

[2]. A. P. Kumar, A. M. Parimi, K. U. Rao, Investigation of small PMSG based wind turbine for variable wind speed, International Conference on Recent Developments in Control, Automation and Power Engineering (RDCAPE), (2015) 107-112.

[3]. C. Wei, Z. Zhang, W. Qiao, L. Qu, An adaptive network-based reinforcement learning method for MPPT control of PMSG wind energy conversion systems, IEEE Transactions on Power Electronics, 31(11) (2016) 7837-7848. DOI: 10.1109/TPEL.2016.2514370.

[4]. A. Urtasun, P. Sanchis, I. San Martin, J. López, L. Marroyo, Modeling of small wind turbines based on PMSG with diode bridge for sensorless maximum power tracking, Renewable energy, 55 (2013), 138-149. https://doi.org/10.1016/j.renene.2012.12.035

[5]. S. Ghosh, N. Senroy, Electromechanical dynamics of controlled variable-speed wind turbines, IEEE Systems Journal, 9(2) (2013) 639-646. DOI: 10.1109/JSYST.2013.2280037

[6]. C. Huang, F. Li, Z. Jin, Maximum power point tracking strategy for large-scale wind generation systems considering wind turbine dynamics, IEEE Transactions on Industrial Electronics, 62(4) (2015) 2530-2539. DOI: 10.1109/TIE.2015.2395384

[7]. V., Petrović, C. L. Bottasso, Wind turbine envelope protection control over the full wind speed range. Renewable energy, 111 (2017) 836-848. https://doi.org/10.1016/j.renene.2017.04.021

[8]. M. Yin, W. Li, C.Y. Chung, L. Zhou, Z. Chen, Y. Zou, Optimal torque control based on effective tracking range for maximum power point tracking of wind turbines under varying wind conditions, IET Renewable Power Generation, 11(4) (2016) 501-510. DOI: 10.1049/iet-rpg.2016.0635

[9]. M. J. Yarmohammadi, A. Sadeghzadeh, M. Taghizadeh, Gain-scheduled control of wind turbine exploiting inexact wind speed measurement for full operating range, Renewable Energy, 149 (2020) 890-901 https://doi.org/10.1016/j.renene.2019.09.148

[10]. W. Markus, E. István, Variable Speed Wind Turbines Based on Electromechanical Differential Systems, IEEE Transactions on Energy Conversion, 29(1) (2014) 101-109. DOI: 10.1109/TEC.2013.2287260.

[11]. F. A. Inthamoussou, H. De Battista, R.J. Mantz, LPV-based active power control of wind turbines covering the complete wind speed range, Renewable Energy, 99 (2016) 996-1007. https://doi.org/10.1016/j.renene.2016.07.064.

[12]. R.C. Lupton, R.S. Langley, Improved linearised models of wind turbine aerodynamics and control system dynamics using harmonic linearization, Renewable energy, 135 (2019) 148-162. https://doi.org/10.1016/j.renene.2018.11.067

[13]. M. Karabacak, A new perturb and observe based higher order sliding mode MPPT control of wind turbines eliminating the rotor inertial effect, Renewable energy, 133 (2019) 807-82. https://doi.org/10.1016/j.renene.2018.10.079

[14]. A. R. Youssef, H. H.Mousa, E. E. Mohamed, Development of self-adaptive P&O MPPT algorithm for wind generation systems with concentrated search area, Renewable Energy, 154 (2020) 875-893. https://doi.org/10.1016/j.renene.2020.03.050.

[15]. J. C. Hui, A. Bakhshai, P.K. Jain, A sensorless adaptive maximum power point extraction method with voltage feedback control for small wind turbines in off-grid applications, IEEE Journal of Emerging and Selected Topics in Power Electronics, 3(3) (2015) 817-828. DOI: 10.1109/JESTPE.2015.2432677

[16]. Y. Bai, B. Kou, C. C. Chan, A simple structure passive MPPT standalone wind turbine generator system, *IEEE Transactions on Magnetics*, *51*(11) (2015) 1-4. DOI: 10.1109/TMAG.2015.2439043

[17]. Y. Wang, J. Meng, X. Zhang, L. Xu, Control of PMSG-based wind turbines for system inertial response and power oscillation damping, IEEE Transactions on Sustainable Energy, 6(2) (2015) 565-574. DOI: 10.1109/TSTE.2015.2394363

[18]. M. Zhang, X. Li, J. Tong, J. Xu, Load control of floating wind turbine on a Tension-Leg-Platform subject to extreme wind condition, Renewable Energy, 151 (2019) 993-1007. https://doi.org/10.1016/j.renene.2019.11.093.

[19]. Y. Yuan, X. Chen, J. Tang, Multivariable robust blade pitch control design to reject periodic loads on wind turbines, Renewable Energy, 146 (2020) 329-341. https://doi.org/10.1016/j.renene.2019.06.136.

[20]. P. Venkaiah, B. K. Sarkar, Hydraulically actuated horizontal axis wind turbine pitch control by model free adaptive controller, Renewable Energy, 147 (2020) 55-68. https://doi.org/10.1016/j.renene.2019.08.127

[21]. M. Narayana, G. A. Putrus, M. Jovanovic, P.S. Leung, S. McDonald, Generic maximum power point tracking controller for small-scale wind turbines, Renewable Energy, 44 (2012) 72-79. https://doi.org/10.1016/j.renene.2011.12.015.

[22]. M.H. Qais, H.M. Hasanien, S. Alghuwainem, A grey wolf optimizer for optimum parameters of multiple PI controllers of a grid-connected PMSG driven by variable speed wind turbine, IEEE Access, 6 (2018) 44120-44128. DOI: 10.1109/ACCESS.2018.2864303

[23]. G. Xu, F. Liu, J. Hu, T. Bi, Coordination of wind turbines and synchronous generators for system frequency control, Renewable energy, 129 (2018) 225-236. https://doi.org/10.1016/j.renene.2018.05.104

[24]. F. J. Madsen, T. R. L. Nielsen, T. Kim, H. Bredmose, A. Pegalajar-Jurado, R.F. Mikkelsen, P. Shin, Experimental analysis of the scaled DTU10MW TLP floating wind turbine with different control strategies, Renewable Energy, 155, (2020) 330-346. https://doi.org/10.1016/j.renene.2020.03.145

[25]. F. Jaramillo-Lopez, G. Kenne, F. Lamnabhi-Lagarrigue, A novel online training neural network-based algorithm for wind speed estimation and adaptive control of PMSG wind turbine system for maximum power extraction, Renewable Energy, 86 (2016) 38-48. https://doi.org/10.1016/j.renene.2015.07.071

[26]. O. Barambones, J.A. Cortajarena, I. Calvo, J. M. G. de Durana, P. Alkorta, A. Karami-Mollaee, Variable speed wind turbine control scheme using a robust wind torque estimation, Renewable energy, 133 (2019) 354-366. https://doi.org/10.1016/j.renene.2018.10.009

[27]. A. Tohidi, H. Hajieghrary, M.A. Hsieh, Adaptive disturbance rejection control scheme for DFIG-based wind turbine: Theory and experiments, IEEE Transactions on Industry Applications, 52(3) (2016) 2006-2015. DOI: 10.1109/TIA.2016.2521354

[28]. S. Abdelmalek, L. Barazane, A. Larabi, M. Bettayeb, A novel scheme for current sensor faults diagnosis in the stator of a DFIG described by a TS fuzzy model, Measurement, 91 (2016) 680–691. https://doi.org/10.1016/j.measurement.2016.05.102

[29]. S. Abdelmalek, L. Barazane, A. Larabi, Fault diagnosis for a doubly fed induction generator, Revue Roumaine des Sciences Techniques-Serie Electrotechnique et Energetique, 61 (2016) 159–163.

[30]. S. Sanchez, M. Molinas, M. Degano, P. Zanchetta, Stability evaluation of a DC micro-grid and future interconnection to an AC system, Renewable Energy, 62 (2014) 649-656. https://doi.org/10.1016/j.renene.2013.08.026

[31]. S. Abdelmalek, L. Barazane, A. Larabi, An advanced robust fault-tolerant tracking control for a doubly fed induction generator with actuator faults, Turkish Journal of Electrical Engineering & Computer Sciences, 25 (2017) 1346–1357. DOI:10.3906/elk-1508-16

[32]. B. Yang, T. Yu, H. Shu, Y. Zhang, J. Chen, Y. Sang, L. Jiang, Passivity-based sliding-mode control design for optimal power extraction of a PMSG based variable speed wind turbine, Renewable Energy, 119 (2018) 577-589. https://doi.org/10.1016/j.renene.2017.12.047

[33]. M.E. Haque, M. Negnevitsky, K. M. Muttaqi, A novel control strategy for a variable speed wind turbine with a permanent magnet synchronous generator, IEEE Transactions on Industry Applications, 46(1) (2010) 331-339. DOI: 10.1109/TIA.2009.2036550

[34]. B. Yang, T. Yu, H. Shu, Y. Han, P. Cao, L. Jiang, Adaptive fractional-order PID control of PMSG-based wind energy conversion system for MPPT using linear observers, International Transactions on Electrical Energy Systems, 29(1) L. (2019) 2697. https://doi.org/10.1002/etep.2697

[35]. K. V. G. Raghavendra, K. Zeb, A. Muthusamy, T. N. V. Krishna, S. V. S. Kumar,D.H. Kim, D. H., H.J. Kim, A Comprehensive Review of DC–DC Converter Topologies and Modulation Strategies with Recent Advances in Solar Photovoltaic Systems. Electronics, 9(1) (2020) 31. https://doi.org/10.3390/electronics9010031

[36]. A. Dali, S. Diaf, M. Tadjine, Maximum Power Tracking and Current Control for Solar Photovoltaic System Applications, Hybrid Dynamical System Approach, Journal of Dynamic Systems Measurement and Control, , 141(9) (2019) 091017-091025. DOI:10.1115/1.4043556

[37]. A. Dali, S. Abdelmalek, M. Bettayeb, A new combined observer-state feedback (COSF) controller of pwm buck converter, The International Conference on Electrical Sciences and Technologies in Maghreb (CISTEM), (2018). DOI: 10.1109/CISTEM.2018.8613454.

[38]. S. Abdelmalek, A. Dali, d M. Bettayeb, An improved observer-based integral state feedback (OISF) control strategy of flyback converter for photovoltaic systems, The International Conference on Electrical Sciences and Technologies in Maghreb (CISTEM), (2018). DOI: 10.1109/CISTEM.2018.8613565

[39]. S. Mensou, A. Essadki, T. Nasser, B.B. Idrissi, L.B. Tarla, Dspace DS1104 implementation of a robust nonlinear controller applied for DFIG driven by wind turbine, Renewable Energy, 147 (2020) 1759-1771. https://doi.org/10.1016/j.renene.2019.09.042

[40]. M. Abolvafaei, S. Ganjefar, Maximum power extraction from wind energy system using homotopy singular perturbation and fast terminal sliding mode method, Renewable Energy, 148 (2020) 611-626. https://doi.org/10.1016/j.renene.2019.10.150

[41]. B. Wang, G. Ma, D. Xu, L. Zhang, J. Zhou, Switching sliding-mode control strategy based on multi-type restrictive condition for voltage control of buck converter in auxiliary energy source. Applied Energy, 228 (2018) 1373-1384. https://doi.org/10.1016/j.renene.2019.10.150

[42]. S. Bendoukha, S. Abdelmalek, S. Abdelmalek, A new combined actuator fault estimation and accommodation for linear parameter varying system subject to simultaneous and multiple faults: an lmis approach, Soft Computing, 23 (2018) 10449–10462. https://doi.org/10.1007/s00500-018-3601-3

[43]. A. Bakdi, A. Kouadri, S. Mekhilef, A data-driven algorithm for online detection of component and system faults in modern wind turbines at different operating zones, Renewable and Sustainable Energy Reviews, 103 (2019) 546-555. https://doi.org/10.1016/j.rser.2019.01.013

[44]. S. Abdelmalek, A. T. Azar, D. Dib, A novel actuator fault- tolerant control strategy of dfig-based wind turbines using Takagi-Sugeno multiple models, International Journal of Control Automation and Systems, 16 (2018) 1415–1424. https://doi.org/10.1007/s12555-017-0320-y

[45]. S. Abdelmalek, A. Dali, A. Bakdi, M. Bettayeb, Design and experimental implementation of a new robust observer-based nonlinear controller for DC-DC buck converters, Energy, 213 (2020), 118816. https://doi.org/10.1016/j.energy.2020.118816.

[46]. S. Abdelmalek, A. Dali, A. Bakdi, M. Bettayeb, A new effective robust nonlinear controller based on PSO for interleaved DC–DC boost converters for fuel cell voltage regulation, Soft Computing, 24 (2020) 17051–17064. https://doi.org/10.1007/s00500-020-04996-4.